

Simulation of tyre rolling resistance generated on uneven road

Wei, Chongfeng; Olatunbosun, Oluremi A.; Behroozi, Mohammad

DOI:

[10.1504/IJVD.2016.074415](https://doi.org/10.1504/IJVD.2016.074415)

License:

None: All rights reserved

Document Version

Peer reviewed version

Citation for published version (Harvard):

Wei, C, Olatunbosun, OA & Behroozi, M 2016, 'Simulation of tyre rolling resistance generated on uneven road', *International Journal of Vehicle Design*, vol. 70, no. 2, pp. 113-136. <https://doi.org/10.1504/IJVD.2016.074415>

[Link to publication on Research at Birmingham portal](#)

General rights

Unless a licence is specified above, all rights (including copyright and moral rights) in this document are retained by the authors and/or the copyright holders. The express permission of the copyright holder must be obtained for any use of this material other than for purposes permitted by law.

- Users may freely distribute the URL that is used to identify this publication.
- Users may download and/or print one copy of the publication from the University of Birmingham research portal for the purpose of private study or non-commercial research.
- User may use extracts from the document in line with the concept of 'fair dealing' under the Copyright, Designs and Patents Act 1988 (?)
- Users may not further distribute the material nor use it for the purposes of commercial gain.

Where a licence is displayed above, please note the terms and conditions of the licence govern your use of this document.

When citing, please reference the published version.

Take down policy

While the University of Birmingham exercises care and attention in making items available there are rare occasions when an item has been uploaded in error or has been deemed to be commercially or otherwise sensitive.

If you believe that this is the case for this document, please contact UBIRA@lists.bham.ac.uk providing details and we will remove access to the work immediately and investigate.

Chongfeng Wei, e-mail: cxw103@bham.ac.uk
Oluremi A Olatunbosun*, e-mail: O.A.Olatunbosun@bham.ac.uk
Mohammad Behroozi, e-mail: mbehroozi718@gmail.com

* Corresponding author

School of Mechanical Engineering
University of Birmingham
Edgbaston
Birmingham
B15 2TT

Simulation of tyre rolling resistance generated on uneven road

Abstract: Due to limitations of laboratory test rigs to reproduce some of the more extreme operating conditions (such as a tire rolling over large obstacles), not all the tire parameters and characteristics can be derived using tire dynamic tests. However, most tire dynamic responses and vibration properties can be virtually simulated using Finite Element analysis which has long been recognized as a significant simulation tool for tire characteristics investigation. The objective of this study is to determine the rolling resistance of a tire rolling on an uneven road by simulating the energy loss in the tire and the longitudinal force. The tire model was developed with detailed geometry and material definition, and satisfactory results were obtained by validation of the transient dynamic response of the tire rolling over obstacles. For simulating a tire rolling on an uneven road, the road unevenness was generated using the Inverse Discrete Fourier Transform method. Finally, the effects of different kinds of road unevenness and different travelling velocities on rolling resistance were investigated.

Keywords: tire, rolling resistance, finite element, simulation, uneven road

1. Introduction

As an important factor in vehicle fuel consumption, tire rolling resistance is being paid more and more attention by researchers since the energy dissipation due to tire rolling resistance is a major component of vehicle energy loss (up to one third of energy consumed by the engine[1]). Rolling resistance is caused by tire deflection and deformation while rolling on the road, and the material hysteresis of tire rubber and the tire structure is the primary contributor to energy dissipation. When the tire is loaded on a flat surface, energy losses occur due to the contact patch being deformed from the original shape in the unloaded condition according to the property and flexibility of the internal tire structure, rubber, sidewall and tread. On the other hand, for the tire rolling on an uneven road, the tread element is deflected in the horizontal direction, and rolling resistance will be generated by the longitudinal force against motion because of the road unevenness. During the last decades, most of the researches have concentrated on the rolling resistance of the tire at steady state conditions. In this paper, special attention is paid to the energy loss generated in the tire due to the longitudinal force resulting from the tire rolling on an uneven road.

Finite element analysis is a useful method for predicting tire properties and parameters instead of tire testing, particularly when test rigs in the laboratory are unable to meet the requirements of certain extreme or special operating conditions, e.g. for the tire rolling on an uneven road or over large obstacles. Over the last twenty years, there have been many researchers using finite element analysis to study the prediction of rolling resistance of tires and energy dissipation. Ebbott et al. [2] demonstrated a semi-coupled finite element-based method to predict rolling resistance and temperature distribution, in which particular attention is paid to the constitutive models and material properties of the tire. Shida et al. [3] proposed a simulation method using static finite element analysis to estimate the energy dissipation based on the relationship between the variation of stresses and strains approximated by Fourier series and the viscoelastic phase lag. In order to achieve adequate accuracy of the rolling resistance prediction, the anisotropic loss factor in fiber-reinforced rubbers was appropriately considered in the tire model. More recently, Ghosh [4] evaluated rolling resistance of a passenger car radial tyre with nanocomposite based tread compounds by using finite element (FE) analysis, in which energy dissipation was obtained for steady state rolling simulation. Cho et al. [5, 6] constructed a detailed periodic patterned tire model to predict the hysteretic loss and rolling resistance making use of the 3-D static tire contact analysis. However, the prediction of rolling resistance from these models was conducted at static or steady-state rolling conditions, while the transient rolling resistance of tires was ignored. In the research of Luchini and Popio [7], an analytical transient tire model was used to predict rolling resistance in which the

model parameters were derived using equilibrium test data. From the comparison of rolling resistance obtained from simulation and measurement, it could be observed that the accuracy of rolling resistance prediction is affected by the different test protocols. In this paper, a detailed 3D tire model is developed from the geometry and material definition, and validated with transient dynamic tests for the physical tire. Finally, the rolling resistance generated by the longitudinal force resulting from the tire rolling on an uneven road is predicted using transient dynamic simulation.

The following are the contributions of this paper: (1) development of a detailed finite element tire model for tire rolling simulation capable of representing the complex structure of the tire, (2) a mathematical method for prediction of rolling resistance generated by the longitudinal forces between the tire and uneven road was developed, and (3) it was shown that the rolling resistance on an uneven road is due mainly to the longitudinal dynamic forces.

For the tire rolling on a flat surface, the contributions of rolling resistance comes from three sources: aerodynamic loss, tire scrubbing, and material hysteresis of components in the tire, with material hysteresis being the primary contributor to rolling resistance of the tire [1, 8]. With tire/road interaction, the original unloaded state of the tire is modified, and the contact patch is deformed from the original shape. The tread rubber will be compressed or stretched depending on the tire/road contact pressure while the sidewall of the tire will bend because of the flexibility of the tire sidewall. Rolling resistance is usually generated in the process of tire component recovery from one position to another position on the flat surface, and most of the rolling loss converts to heat. Different Researchers have used different methods to describe and calculate rolling resistance. Clark [8] described the concept of rolling resistance as a function of inflation pressure and vertical load according to the equally linear relationship between normalised rolling resistance and these two factors. Pillai [9] also developed a general equation for rolling resistance in terms of tire load at constant inflation pressure. The concept of rolling resistance of a tire is usually expressed in the form of energy dissipated divided by distance travelled. In the study of Shida et al. [3], energy dissipation is evaluated through the relationship between variation of stress and strain energy and the viscoelastic phase lag of tire rubber. The widely used numerical approaches to calculating the hysteretic loss and rolling resistance are by approximating the time histories of strains during one revolution in steady state rolling [5].

For a tire rolling on an uneven road or traversing obstacles on the road, however, calculating the energy loss cannot be carried out using the traditional methods applied in the case of a tire rolling on a flat surface. Energy dissipation in a tire rolling on an uneven road consists of various components of the tire's strain energy such as

the energy dissipated through inelastic processes such as plasticity, the energy dissipated through viscoelasticity or creep, the energy dissipation because of tire/road sliding friction, and the fluid cavity energy. On the other hand, the energy dissipation generated by the longitudinal force because of the road unevenness is another principal component of energy loss, which could be classified as energy dissipation from external work, and is the main subject of this study.

2. Materials and Method

2.1 Finite Element tire model

Figure 1(a) illustrates half of the 2D cross section of a 235/60 R18 tire model, and the FE model was built and computed using ABAQUS 6.12. According to the material categories, the tire components are classified as two parts: rubber components and reinforcements. The rubber components are composed of tread, inner liner, sidewall and apex, which are defined with solid elements, while the reinforcements consist of one carcass layer with double ply polyester, one cap ply, two steel belts and several bead cords, which are modelled with rebar in surface elements (Figure 1(a)). All the material properties of the tire components defined in ABAQUS were obtained using a combination of curve fitting of experimental tests and numerical modelling in finite element simulation. The three-dimension tire model is obtained by revolving the 2D cross section of the tire about the rotational symmetric axis, which is illustrated in Figure 1 (b). In the FE model, the road was defined as an analytical rigid surface since the road stiffness is usually much higher than the stiffness of the tire. Tire/road contact was specified by three constraints: 1) the tire and road cannot penetrate into each other in the process of movement, 2) only pressure composes the normal component of contact force, 3) friction is generated in the tangential direction between tire and road (the friction coefficient was set as 1.0). In this study, the penalty contact method was used to enforce contact in the normal direction, and Coulomb model of friction was adopted to define the tangential contact constraint.

In this study, a 235/R18 tire was cut in order to obtain the geometry information of the tire. Based on the researches of vehicle dynamics research group of University of Birmingham [11-15], the image of the tire's cross section was captured using a high resolution camera, and then image processing methods were used to further process the image of the cross section in order to satisfy the FE modelling requirements.

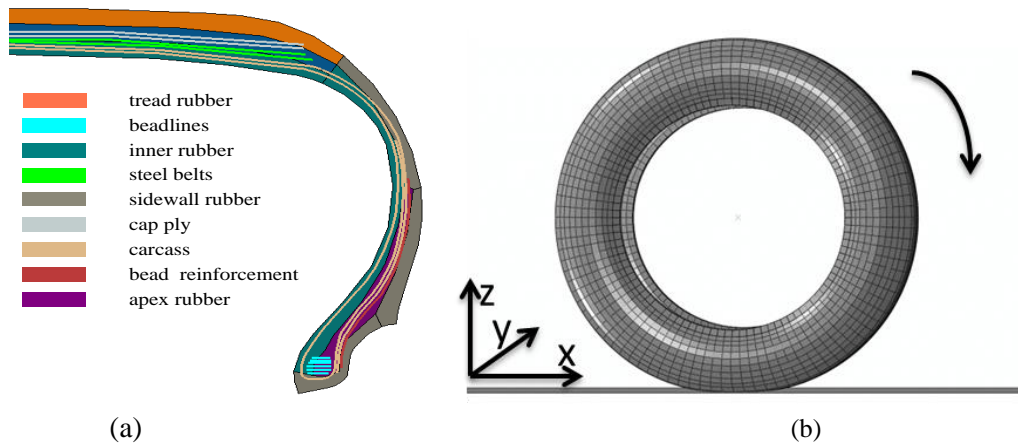


Figure 1. (a) Components of 2D tire cross-section model, (b) the revolved 3D tire model

As mentioned above, the material properties of rubber components and reinforcements of the tire are defined by experimental tests and computational processing, thus the specimens of rubber components and reinforcements of the tire need to be extracted from the tire product. Rubber components of a tire in finite element analysis are represented using the hyperelastic model and viscoelastic model to describe the properties of rubber material, and the properties of reinforcements are represented by parallel layers of unidirectional rebar elements with isotropic material properties. In this study, the Yeoh model [10] was applied to define the hyperelastic property of rubber components. The reason for using the Yeoh model in the tire rubber material model is described in detail in the following paragraph.

With review of a number of elasticity models of rubber material, which are used to describe the hyperelastic property, it is found that most of these models are determined based on the polynomial expression of strain energy function. Among these material hyperelastic property models, Mooney-Rivlin energy density function has been widely applied for tire dynamic properties analysis in the finite element simulation [16, 17]. However, the Mooney-Rivlin function has a limitation that it could not be accurately applied to large deformation problems of the rubber material [18]. In order to determine the parameters of rubber hyperelastic property, most of the material models need to combine three deformation tests (uni-axial, biaxial tension and pure shear), which is recognized as a complex and time consuming procedure. Although Neo-Hookean material model is supported in ABAQUS [19], it also has a limitation that the coefficients derived from uni-axial deformation tests are not suitable to describe other deformation modes. Ogden strain energy function derived from stress-strain data obtained from one deformation mode is also unsatisfactory for predicting rubber behaviour in other modes [20]. The Yeoh hyperelastic material model is not only suggested and supported in ABAQUS, but is also capable of

predicting different deformation modes using data from a simple deformation mode like uni-axial tension test [13].

According to the requirements of rubber test methods in ASTM-D412 [21], the rubber specimens were extracted from the tire product and uni-axial tension tests were carried out by stretching the specimens up to 100% strain at the velocity of 50 mm/min. The data of relationship between tensile stress and strain was recorded. In order to obtain accurate test data, the samples were stretched at least three times to acquire the average values. ABAQUS provides different evaluation functions to fit the test data and determine the material model constants. Figure 2 shows the fitting process for the tread rubber using different hyperelastic material evaluation functions.

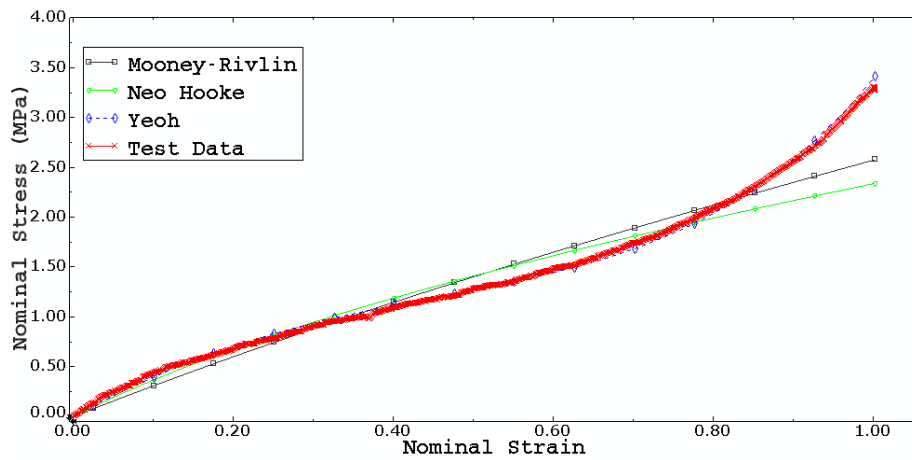


Figure2.Hyperelasticity evaluation with different material models

By the consideration of the material model accuracy and test rig simplicity and time, the Yeoh model has been chosen to define the hyperelastic property of the rubber in tire models. The strain energy function is presented in terms of Equation 1.

$$U = C_{10} (I_1 - 3) + C_{20} (I_1 - 3)^2 + C_{30} (I_1 - 3)^3 + \frac{1}{D_1} (J^{el} - 3)^2 + \frac{1}{D_2} (J^{el} - 3)^4 + \frac{1}{D_3} (J^{el} - 3)^6 \quad (1)$$

where U represents the strain energy density; C_{i0} and D_i are material constants to be determined by testing and test data fitting in ABAQUS, which describe the shear behaviour and material compressibility separately; J^{el} is the elastic volume ratio, while I_1 is the first deviatoric strain invariant. Based on the uni-axial test results and the procedure of material model evaluation, the Yeoh model constants for different rubber components are shown in Table 1. It is noted that D_i ($i=2,3$) was set equal to zero since rubber is assumed to be a fully incompressible material.

Table 1. Hyperelastic model constants

Rubber Material	Yeoh strain energy potentials constants					
Component	C10	C20	C30	D1	D2	D3
Tread	0.7303	-0.1794	7.9572E-02	2.76E-02	0	0
Sidewall	0.7064	-0.2817	0.1323	2.85E-02	0	0
Apex	1.2763	-1.2522	1.2027	1.58E-02	0	0

Viscoelastic property, in conjunction with hyperelastic property of the rubber material, is also considered in this paper. The viscoelastic property of the material provides a more accurate representation of the real world rubber behaviour, and the finite element model should include consideration of this characteristic. Stress-relaxation tests were carried out to define the viscoelasticity in the time domain by using the samples extracted from tire rubber components. The same specimens used in hyperelastic property tests were used for the relaxation tests. Different from the hyperelasticity tests, the specimens were stretched to a constant strain level (up to 50%) and kept for 950 seconds, stress values at different time intervals were recorded. This test was repeated three times to determine the average stress relaxation curve. The viscoelastic material property response is defined in the time domain in ABAQUS by a Prony series expansion of the dimensionless relaxation modulus which can be represented as follows [19]

$$g_R(t) = 1 - \sum_{i=1}^{Na} \overline{g}_i^p (1 - e^{-t/\tau_i^G}) \quad (2)$$

where Na , \overline{g}_i^p and τ_i^G represent material constants to be determined by modelling the physical test in ABAQUS. The evaluation process to fit the normalized relaxation test data of tread rubber using Prony series is illustrated in Figure 3. And the constants of viscoelastic model for different rubber components are shown in Table 2.

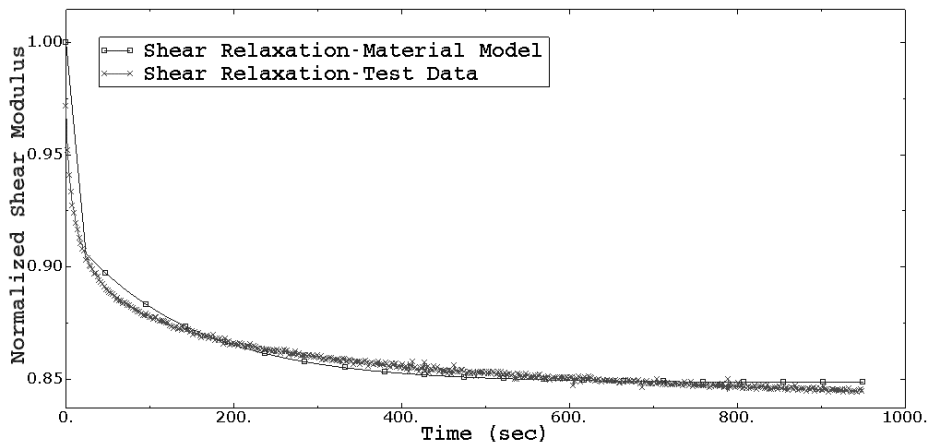


Figure 3. Viscoelasticity evaluation process

Table 2. Viscoelastic model constants for different rubber components

Rubber Material	Prony series parameters			
Component	g_1	τ_1	g_2	τ_2
Tread	0.084	2.39E-5	0.068	142.83
Sidewall	0.098	2.07E-6	0.067	146.11
Apex	0.152	5.76	0.080	220.41

2.2. Steps for calculation of rolling resistance

In this study, the origin of the coordinate system was set at the starting point of rolling, while the x, y and z directions represent the tire travelling direction, lateral direction, and vertical direction respectively, as illustrated in Figure 1(b). The procedure for calculating rolling resistance generated is as follows:

- (1) Construct a random uneven road for definition of the road roughness
- (2) Define the traveling distance (L) of the tire on the uneven road.
- (3) Extract longitudinal forces ($F_x(i)$) against the motion in every time increment during simulation.
- (4) Extract tire traveling displacement ($U_x(i)$) in x direction in every time increment.
- (5) Calculate energy loss (E_d) from external work in the traveling direction.
- (6) Calculate rolling resistance (RR) generated by the longitudinal forces.
- (7) Extract the effective rolling resistance ($RR|_e$) from rolling resistance variation, which is the objective of this study.

Energy loss in a tire, because of the road unevenness, results from external work against tire motion in the longitudinal direction. The difference between rolling velocity and traveling velocity leads to the generation of a longitudinal force. The energy loss from external work can be considered as work done against tire motion in every time increment. Hence the energy loss due to the uneven road is given by the work done by the longitudinal force opposing motion:

$$E_d = \sum |F_x(i)| \cdot U_x(i) \quad (3)$$

In the process of a tire rolling at a constant traveling velocity v on the uneven road and the tire loses the state of free rolling, the situation where $\omega \cdot r < v$ (where ω is the angular velocity and r is the rolling radius) results in a negative longitudinal force, while the situation where $\omega \cdot r > v$ results in a positive longitudinal force. However, both the negative and positive longitudinal forces have the effect of disturbing tire rolling from the

free rolling state, which means both the longitudinal forces in positive x direction and negative x direction generate energy dissipation.

The rolling resistance force can be defined as the energy dissipated in unit distance travelled, which can be presented as follows

$$RR = \frac{E_d}{L} = \frac{E_d}{\sum U_x(i)} \quad (4)$$

2.3. Transient dynamic tire model

2.3.1 Material damping

For the tire traversing an obstacle, the tire model often has a severe numerical oscillation in finite element simulation after the tire rolls over the obstacle at high speed. The road unevenness can be described as consisting of a series of obstacles on the road. Unfortunately viscous damping was unable to effectively control high frequency vibration resulting from the tire rolling over obstacles in FE explicit dynamic simulation. Therefore reasonable convergence of transient dynamic forces could not be achieved without applying material damping. Therefore material damping was introduced to eliminate the numerical oscillation in order that the explicit simulation can reflect the real world behaviour of a tire running on the uneven road. This was introduced in the form of Rayleigh damping for the rubber material. The normal Rayleigh damping matrix is in the following form [22]:

$$[C] = [M] \sum_{k=0}^{p-1} \alpha_k \left([M]^{-1} [K] \right)^k \quad (5)$$

where $[M]$, $[K]$ and $[C]$ are, respectively, the inertial mass, the stiffness matrix, and the viscous damping. The simplest case of this is for proportional damping consisting of only two terms of the normal formula:

$$[C] = \alpha_0 [M] + \alpha_1 [K] \quad (6)$$

As the inertial mass and the stiffness matrix of the system are integrated by their element matrix and vectors [23]:

$$[M] = \sum_e [M^e] \quad [K] = \sum_e [K^e] \quad (7)$$

In which

$$[M^e] = \int_{V_e} \rho [Nc]^T [Nc] dV \quad [K^e] = \int_{V_e} [B]^T [D][B] dV \quad (8)$$

where $[Nc]$ represents the interpolation function matrix, $[B]$ represents the strain matrix, $[D]$ is the elasticity matrix, and ρ is the material density.

According to Equation (5), the material damping matrix can be written as

$$[C] = \alpha_0 \sum_e \int_{V_e} \rho [Nc]^T [Nc] dV + \alpha_1 \sum_e \int_{V_e} [B]^T [D] [B] dV \quad (9)$$

The derivation of Rayleigh damping parameters obtained through vibration tests of rubber samples has been reported in [24], and the values used in this study are $\alpha_0 = 3.7$ and $\alpha_1 = 0.0001$.

In the explicit dynamic analysis, the stable time increment is in proportion to the critical damping for the frequency of the highest mode in the tire model, which is given by

$$\Delta t \approx \sqrt{1 + \xi_{\max}^2} - \xi_{\max} \quad (10)$$

in which ξ_{\max} denotes the critical damping for the highest mode.

2.3.2 Transient dynamic validation of the tire model

In order to effectively predict rolling resistance because of longitudinal responses in the transient dynamic state, it is necessary to validate the tire transient dynamic behaviour. Due to the limitation of laboratory conditions, testing the tire rolling on random uneven road could not be carried out. However, the transient dynamic responses of the tire traversing different obstacles can be validated by the comparison between experimental test and numerical simulation. In addition, the uneven road can be considered as the combination of different kinds of obstacles. In this study, the numerical simulations of the tire rolling over different heights of rectangular obstacles were carried out, in which the height of the tire is fixed and three obstacles with a width of 25mm and heights of 10mm, 20mm, and 25mm were adopted in the study. Both simulation and test were carried out at a velocity of 30km/h and inflation pressure of 200 kPa. The cleat test for model validation was carried out at 30 km/h to limit the impact force on the rig in order to prevent damage to the load cells. Figure 4, Figure 5 and Figure 6 illustrate transient dynamic responses of the tire rolling over three different obstacles, in which satisfactory results were obtained by comparison between numerical simulations and the measurements.

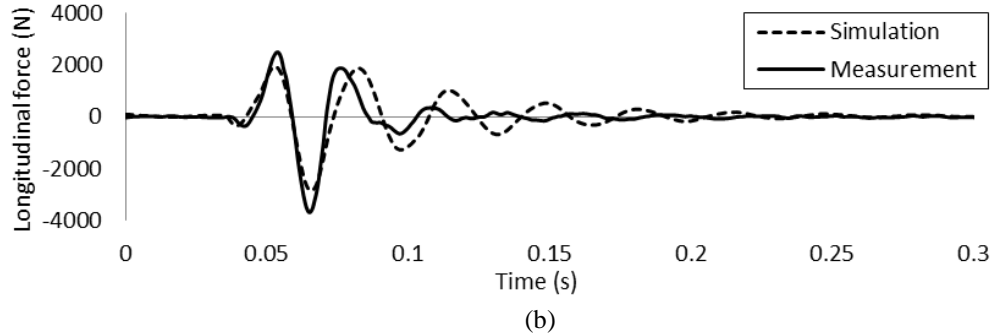
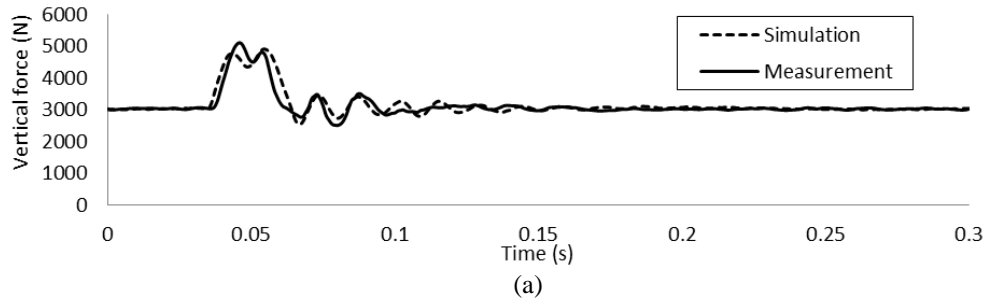


Figure 4. (a) vertical spindle force for tire rolling over 25mm x 10mm obstacle, (b) longitudinal spindle force for tire rolling over 25mm x 10mm obstacle

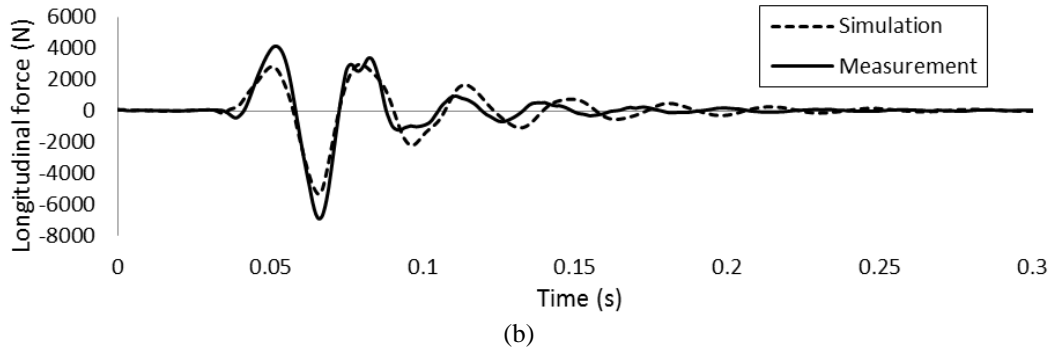
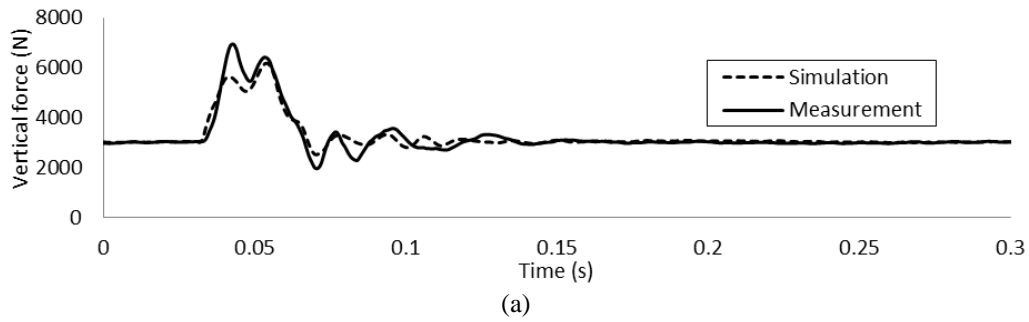
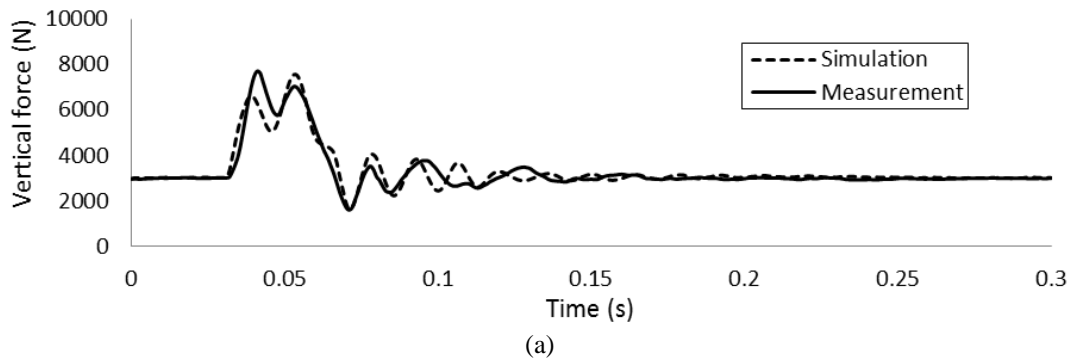


Figure 5. (a) vertical spindle force for tire rolling over 25mm x 20mm obstacle, (b) longitudinal spindle force for tire rolling over 25mm x 20mm obstacle



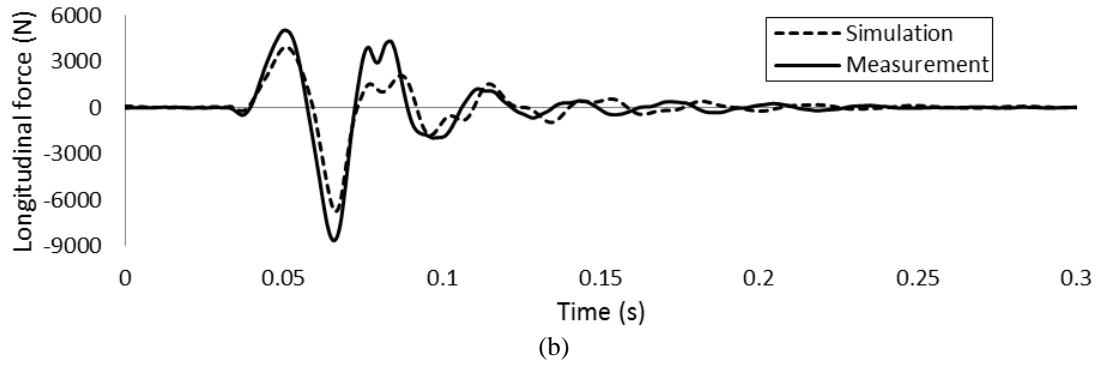


Figure 6. (a) vertical spindle force for tire rolling over 25mm x 25mm obstacle, (b) longitudinal spindle force for tire rolling over 25mm x 25mm obstacle

2.4. Rolling resistance prediction

2.4.1 Road unevenness derivation

Road unevenness has been created to investigate the deformation, dynamic response and enveloping properties in terms of obstacles and steps [26-30]. As a source of excitation for rolling tires, road unevenness is the primary contributor to tire vibration as well as vehicle vibration. In the full vehicle simulation, road unevenness is one of the important input parameters for vehicle dynamic simulation [30]. In this study, braking and traction are not considered, and road unevenness is the main factor that deflects the tire from the free rolling state, and then rolling loss is generated because of the resulting longitudinal forces. Figure 7 illustrates the schematic representation of the contact between the tire and the uneven road. The generated road unevenness data was imported into the FE model for tire rolling analysis.

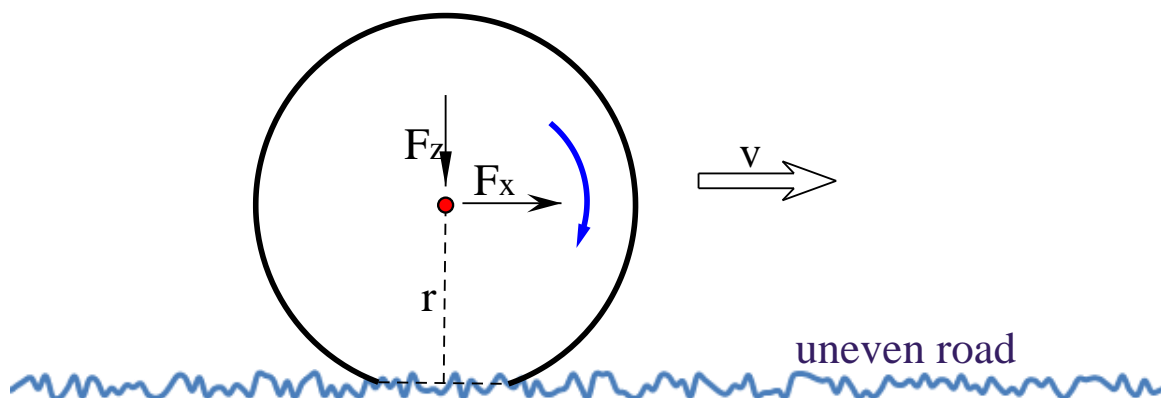


Figure 7. Representation of tire rolling on uneven road

2.4.1.1 Power spectral density of road unevenness

In early studies on vehicle ride performance, the road unevenness was used in the form of sine waves, triangular waves and step functions [31]. However, this simple form of road profiles could not serve as a valid

basis for studying vehicle dynamic performance. Later random functions were introduced to realistically describe the road profiles [31]. When the road profile is recognized as a random function, it can be characterized by a power spectral density function. It has been found that the road unevenness related to the power spectral density for the road profiles can be approximated by [31]

$$S_x(\Omega) = C_{sp} \Omega^{-N_b} \quad (11)$$

in which Ω is the spatial frequency, $S_x(\Omega)$ ($\text{m}^2/\text{cycle}/\text{m}$) is the power spectral density function of the elevation of the road profile, C_{sp} and N_b are dimensionless road profile constants to determine the road unevenness. In order to carry out time domain conversion for road profiles, the power spectral density is expressed in terms of time frequency, which is given by

$$S_x(f) = C_{sp} v^{N_b-1} f^{-N_b} \quad (12)$$

Where v is the travelling velocity of the vehicle, f is the time frequency, and the unit of the power spectral density function $S_x(f)$ is m^2/Hz .

Different road surfaces with different road profile constants are given in table 3, and the power spectral density for different road surfaces is illustrated in Figure 8.

Table 3. Values of N_b and C_{sp} for different PSD functions for various road surfaces [31]

Road surfaces	N_b	C_{sp}
Smooth runway	3.8	4.3×10^{-11}
Rough runway	2.1	8.1×10^{-6}
Smooth highway	2.1	4.8×10^{-7}
Highway with gravel	2.1	4.4×10^{-6}

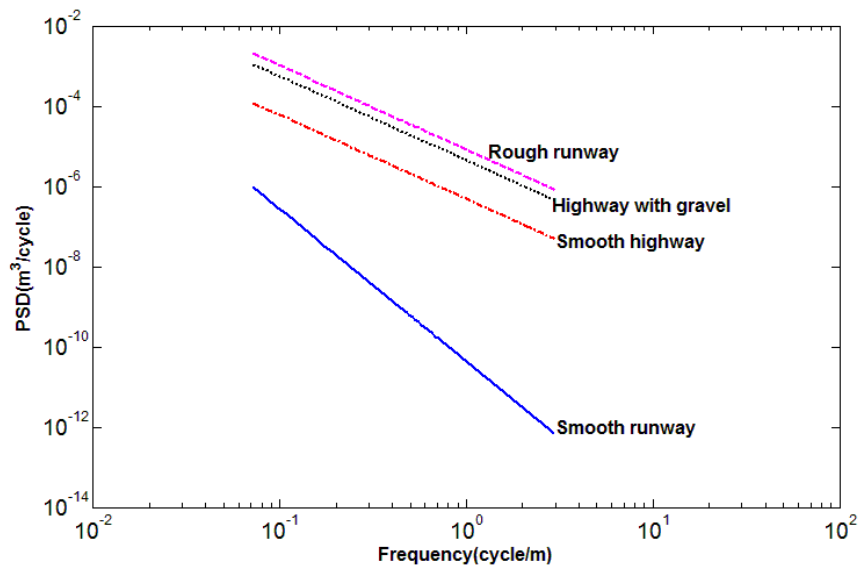


Figure 8. Power spectral density as a function of spatial frequency for various types of road surfaces

2.4.1.2 Discrete Fourier Transform Method

The objective of Discrete Fourier Transform (DFT) is to build the relationship between the time sequence $x(n)$ and the frequency sequence $X(k)$ [32], which can be given by

$$\text{DFT} \quad X(k) = \text{DFT}[x(n)] = \sum_{n=0}^{N-1} x(n) e^{-j\frac{2\pi}{N}nk} \quad k = 0, 1, 2, \dots, N-1 \quad (13)$$

$$\text{IDFT} \quad x(n) = \frac{1}{N} \sum_{k=0}^{N-1} X(k) e^{j\frac{2\pi}{N}nk} \quad k = 0, 1, 2, \dots, N-1 \quad (14)$$

in which N represents the length of the two sequences.

Generally, the definition of power spectral density for a road profile is limited in $(0, +\infty)$ in the DFT process, the one-sided PSD $S_x(f)$ needs to be transformed to the two-sided PSD $G_x(f)$. Based on the characteristics of real even function $G_x(f)$, the power spectral density, the relationship between $S_x(f)$ and $G_x(f)$ can be given by

$$S_x(f) = \begin{cases} 2G_x(f) & f \geq 0 \\ 0 & f < 0 \end{cases} \quad (15)$$

and according to the definition of power spectral density, $S_x(f)$ can be expressed by

$$S_x(f) = \lim_{T \rightarrow \infty} \frac{2}{T} |X(f)|^2 = \lim_{T \rightarrow \infty} \frac{2}{T} \left| \int_{-\infty}^{+\infty} x(t) e^{-j2\pi ft} dt \right|^2 \quad (16)$$

in which t is the simulation time, T is the period, $x(t)$ is the time sequence, and $X(f)$ is the corresponding sequence in terms of frequency. When $t > 0$ and the period T is limited, the Equation (16) can be written as

$$S_x(f) = \frac{2}{T} |X(f)|^2 = \frac{2}{T} \left| \int_0^T x(t) e^{-j2\pi ft} dt \right|^2 \quad (17)$$

By applying DFT on the above equation, associated with eq. 13 and eq. 14, the power spectral density can be derived as

$$S_x(f_k) = \frac{2}{N\Delta t} \left| \sum_{n=0}^{N-1} x(n) e^{-j2\pi f_k n \Delta t} \Delta t \right|^2 = \frac{2\Delta t}{N} |X(k)|^2 = \frac{2T}{N^2} |X(k)|^2 = \frac{2}{\Delta f N^2} |X(k)|^2 \quad (18)$$

in which Δt is the time increment, $N = T / \Delta t$, $\Delta f = 1 / N\Delta t$ and $f_k = k\Delta f$. Therefore, according to the relationship between power spectral density and the time sequence, the frequency sequence can be obtained by

$$|X(k)| = |DFT[x(n)]| = N\sqrt{S_x(f_k)\Delta f / 2} = N\sqrt{S_x(f = k\Delta f)\Delta f / 2} \quad (k = 0, 1, \dots, N_r - 1) \quad (19)$$

The time sequence can be obtained by taking the inverse discrete Fourier transform function (eq. 14) on the above frequency sequence. Based on the above method, the road surface elevations for various types of road

surfaces are obtained (Figure 10), in which the travelling velocity was set as 20km/h, and frequency range within [0.5Hz, 25Hz] was adopted for the simulation.

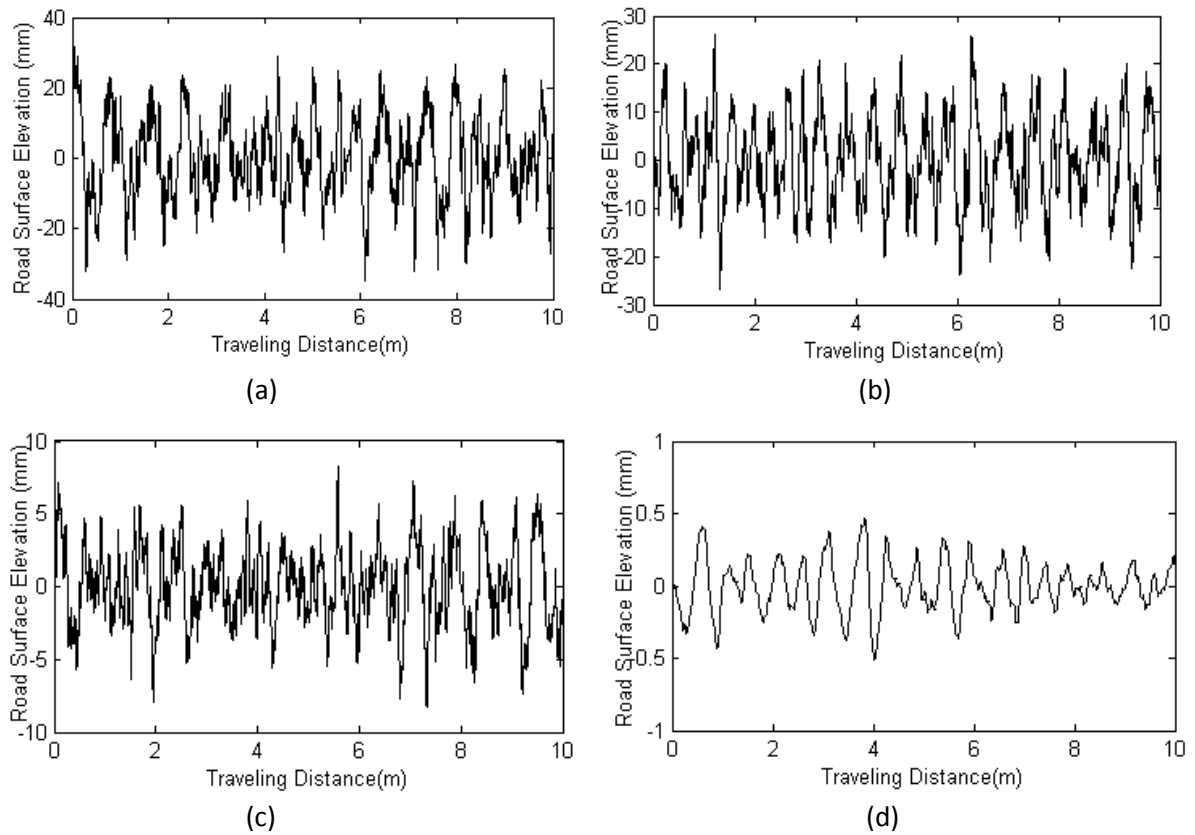


Figure 10. Road unevenness in time domain (a) Rough runway (b) Highway with gravel (c) Smooth highway (d) Smooth runway

The road profiles represented in Figure 10 are 2-D profiles based on the "average" PSD contained in the road unevenness. The 3-D real road profile is randomly uneven, not only in the longitudinal direction but also in the transverse direction. However, the longitudinal force generated over the tyre/road contact patch width is calculated using the 2-D longitudinal profile by integrating over small elements of track width across the width of the contact patch. For each track element the longitudinal force is determined from the local vertical force per unit width. Hence the total longitudinal force over the tyre/road contact patch is obtained by summing over small elements of track width across the width of the tyre.

2.4.2 Quarter car model

The importance of improving dynamic behaviour is growing in vehicle research and development, particularly for the prediction of tire and suspension dynamics properties in rolling over road irregularities, which is important for evaluation of ride comfort in the real driving conditions [33]. Besides, the quarter car model has been used for investigation of chaotic vibration excited by road unevenness [34]. In this study, a quarter car

model consisting of a Finite Element tire and suspension system was built to predict the tire dynamic properties for tire rolling on an uneven road, with a view to deriving the rolling resistance generated by the longitudinal dynamic responses on the uneven road. The quarter car model consists of three components: a tire with an initial condition of contact with the flat road, a chassis which is located above the tire, a suspension composed of spring and dashpot in parallel connecting the chassis and the centre of the tire. In order to achieve a vertical load of 3000N, the weight of the chassis in the finite element model is set as 306kg, and the acceleration due to gravity is set as 9.8 m/s^2 . The schematic representation of the quarter car system is illustrated in Figure 10.

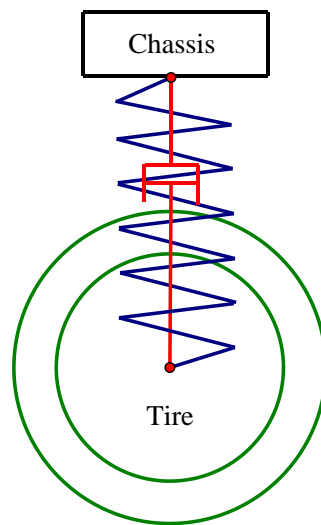


Figure 10. Schematic representation of the quarter car model

2.4.3 Road length

The total length of the road for tire rolling is constructed in three sections: the flat length where the road is assumed to be flat (no excitation), the transition length where there is a transition from no excitation to excitation by the road roughness and the calculation length over which the effective rolling resistance is calculated, as shown in Figure 11. The flat length is created in order that the chassis of the quarter-car can reach an equilibrium position before the tire moves on to the uneven road. As different rolling velocities will generate different travelling distances over which the chassis achieves an equilibrium position, the flat length is calculated based on the travelling velocities.

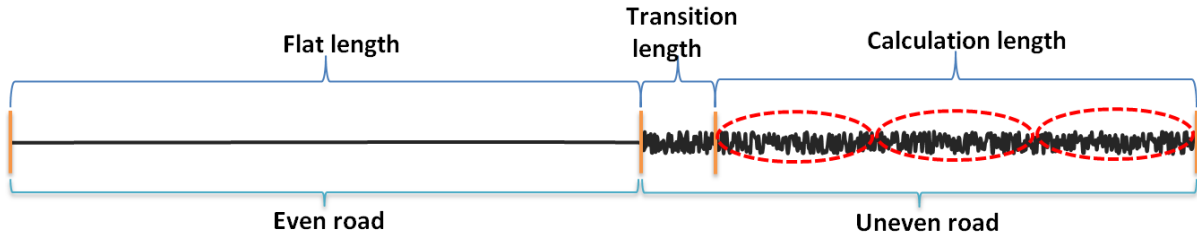


Figure 11. Road length composed of different sections

As mentioned above, the determination of the length of flat road is based on the travelling velocities. Thus, it is important to calculate the equilibrium settling point in the longitudinal direction with different travelling velocities in order that the quarter car system achieves steady state. The travelling time or distance for the tire to achieve a settled state is determined by how long it takes for the system to reach a tolerance band around the final value of vertical displacement [35]. In this study, the permissible zone is set as less than 5% of preload displacement. Figure 12 illustrates the chassis vibration history for the tire travelling at a velocity of 30km/h. The chassis preloading process can be considered as a damped vibration, and the equilibrium position displacement can be estimated as:

$$d = mg / k \quad (20)$$

with m , g , k being the mass of the chassis, gravity acceleration, and suspension stiffness respectively.

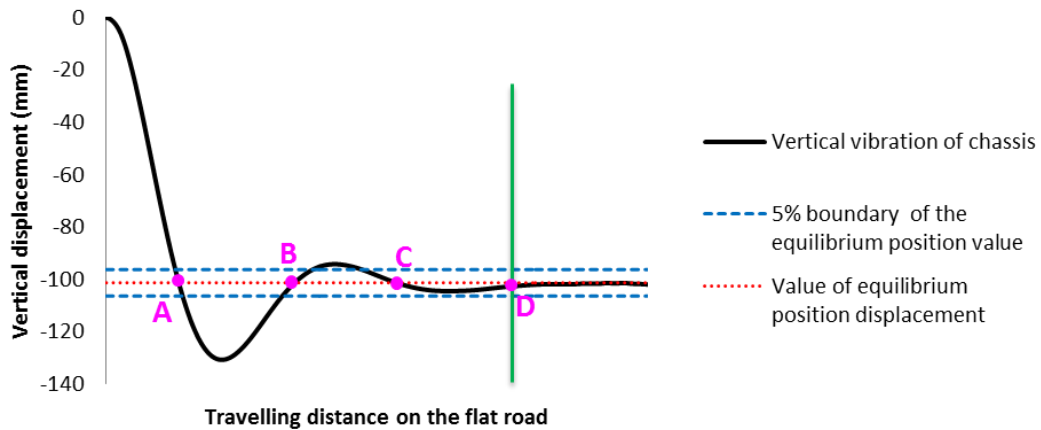


Figure 12. Preloading history of the chassis to get stability for the quarter car model

As shown in Figure 12, the chassis vibration system achieves stability before the D point, which is the fourth crossing point of the vertical displacement curve and the axis of equilibrium. The settling travelling distance at point D meets the requirement of the permissible zone of the vertical displacement. Therefore, the flat length for tire rolling can be determined between the beginning of the road and the perpendicular shown in Figure 12. The

lengths of flat road for travelling velocities of 60km/h and 90km/h are defined by using the same approach as that of 30km/h, and the relationship between the flat length and travelling velocity is illustrated in Figure 13, from which it can be observed that the flat length and the travelling velocity have a nearly linear relationship with each other.

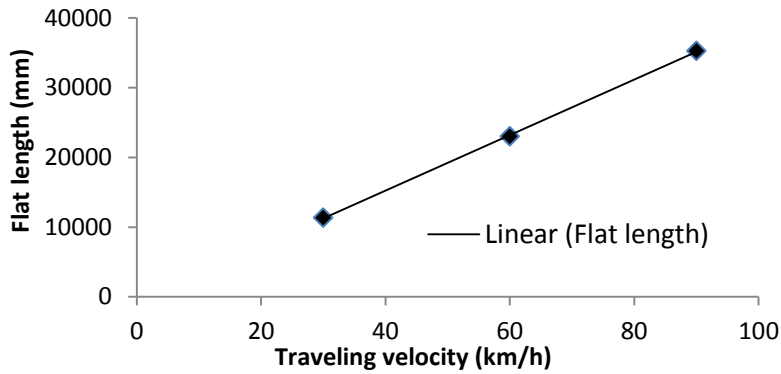


Figure 13. Flat length variation for different travel velocities

With regard to the transition length, it is a required section of uneven road for the rolling resistance to build up to a steady level before it is measured, to ensure accurate rolling resistance results. Figure 14 illustrates the relationship between rolling resistance and distance travelled by the tire on one of the uneven roads at 90km/h. The objective of defining a transition length is to determine the starting position for calculation of rolling resistance accurately. As shown in Figure 14, the initial value of rolling resistance is much lower than that in the future rolling distances, the reason being that the model needs to build up the rolling resistance when the tire moves on to the uneven road, and then rolling resistance reaches a fairly steady value. The perpendicular shows the end of transient length, at which position the rolling resistance reaches a steady value, and the calculation length starts after the perpendicular.

As the most important length of the three parts of road length, the calculation length is applied for calculation of rolling resistance, which is the objective of this study. In order to improve the accuracy of rolling resistance calculation on the uneven road associated with requirement of covering different characteristics of the random road, the rolling resistance is calculated over a minimum of three revolutions of rolling tire on the uneven road. The total distance of the tire rolling over three revolutions was applied for the rolling resistance calculation, which is illustrated in both Figure 11 and Figure 14, and the calculation length can be considered as the effective length.

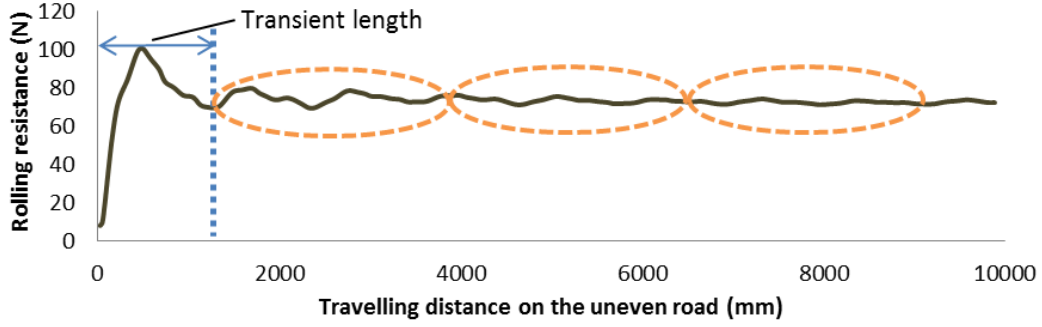


Figure 14. Rolling resistance variation for the tire rolling on the uneven road at 90km/h

2.4.4 Rolling resistance calculation

As mentioned, the calculation length is applied for the calculation of effective rolling resistance. However, the starting point for rolling resistance calculation is the beginning of the uneven road, which consists of the transition length plus the calculation length. As described in Equation 4, for a tire rolling over a distance L of the uneven road, the rolling resistance for this part of the uneven road is calculated in terms of

$$RR|_{0 \rightarrow L} = \frac{E_d}{L} = \frac{E_d}{\sum U_x(i)} \quad (21)$$

in which the $RR|_{0 \rightarrow L}$ represents the average rolling resistance for the tire traversing a distance L of the uneven road. Figure 14 illustrates the rolling resistance variation of the whole uneven road. However, the effective rolling resistance is obtained by extracting the rolling resistance in the distance covered in three revolutions of the tire and calculating the average value of the rolling resistance for this distance. Based on Equation 21, the equation for the effective rolling resistance $RR|_e$ can be written as

$$RR|_e = \frac{RR_1 + RR_2 + RR_3}{3} \quad (22)$$

where RR_1, RR_2, RR_3 represent the rolling resistance for revolution 1, revolution 2 and revolution 3, respectively.

3. Results and Discussion

3.1. Sensitivity of rolling resistance to travelling velocity

As the transition distances for different travelling velocities are different from each other, the definition of the transition length used for the study of comparison of rolling resistance for different travelling velocities was derived by the longest transition length in order that the effective rolling resistance derivation is based on the

same road unevenness and the same calculation length. The rolling resistance variations for different travelling velocities are shown in Figure 15, in which the perpendicular represents the dividing line between transition length and calculation length. Three revolutions behind the perpendicular were selected as the calculation length to evaluate the effective rolling resistance.

The calculation of the end position of the third revolution of rolling tire is determined by the rotational displacement of the tire rim. Figure 16 describes the corresponding rotational displacement variation with the increase of travelling distance of the tire rolling on the uneven road for the travelling velocity of 30km/h. With the relationship between rotational displacement of the rim and the tire travelling distance on the uneven road, in which the perpendicular illustrated is applied for determining the corresponding position with the starting position of the calculation length, the calculation length can be conveniently determined by extracting the section between the two positions. Although different travelling velocities were applied in the simulation, the methods of applying rotational displacement to evaluate the three revolutions section for the three travelling velocities were consistent with each other. Hence the end position of the third revolution of the rolling tire is the same for the other two different travelling velocities.

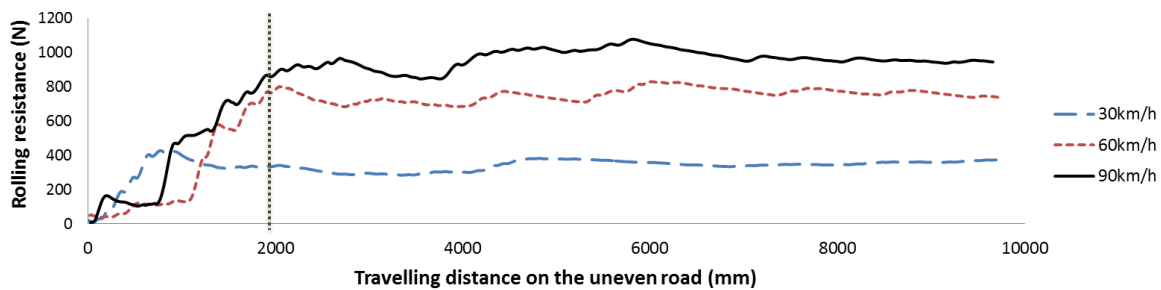


Figure 15. Rolling resistance variation with the increase of travelling distance of the uneven road

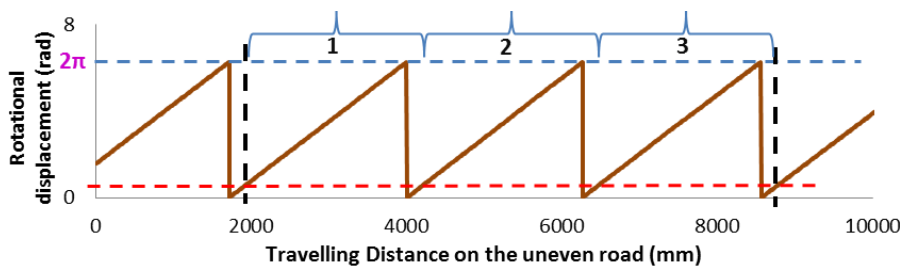


Figure 16. The corresponding rotational displacement variation with the increase of travelling distance of the uneven road for the travelling velocity of 30km/h

The effective rolling resistances for different travelling velocities can be derived according to Equation. 29.

The relationship between rolling resistance and travelling velocities were derived and illustrated in Figure 17.

Different travelling velocities of 30km/h, 60km/h, and 90km/h associated with an inflation pressure of 200kPa were set as operating conditions and applied for rolling simulation for investigation of the influence of travelling velocities on rolling resistance. The rolling resistances generated on uneven road because of longitudinal forces for different travelling velocities are shown in Figure 17. It can be observed that, with regard to rolling resistance because of road unevenness, higher travelling velocity leads to higher rolling resistance.

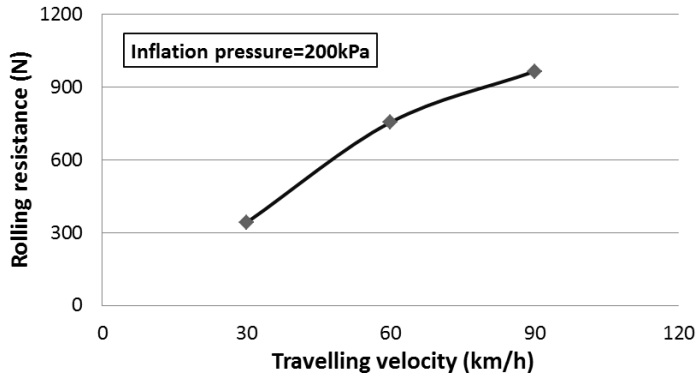


Figure 17. Effective rolling resistance variations for the quarter car model at different travelling velocities

3.2 Sensitivity of rolling resistance to road surface level

In order to investigate the effect of road roughness on rolling resistance, two typical road surfaces, the smooth runway and rough runway, mentioned in the previous section were chosen for rolling resistance analysis. In this study, coefficient of rolling resistance is applied to make the comparison between different road surfaces. The coefficient of rolling resistance is the standard way of expressing rolling loss of the rolling tire and is defined as the ratio of the rolling resistance to the normal load. Various empirical formulas have been developed based on experimental results for calculating the rolling resistance of tires on hard surfaces. Rolling resistance coefficient for a radial-ply tire may be expressed as [31]:

$$f_r = 0.0136 + 0.40 \times 10^{-7} V^2 \quad (23)$$

where V is the vehicle speed in km/hr.

The rolling resistance coefficient of a tire on a hard surface is due mainly to the hysteresis loss in the tire due to deformation as it rolls. Here, the rolling resistance coefficients from numerical simulation for the two kinds of road surfaces are compared to that for a hard surface in Figure 17 for different travelling velocities. It can be observed that the rolling resistance coefficient for the uneven surface is much higher than that of the smooth surface (calculated from Equation 23), indicating that the rolling resistance for an uneven surface is mainly due to the transient longitudinal contact forces generated at the tire-pavement interface.

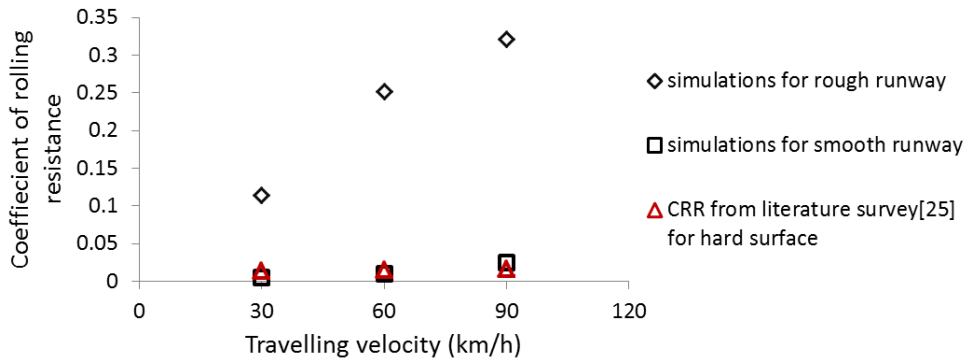


Figure 18. Variation of Coefficient of rolling resistance with the increase of travelling velocities for the two conditions in comparison to smooth road.

In the BOSCH automotive handbook [36], the average measured values of the coefficient of rolling resistance for various types of road surfaces are shown in Table 4. The average measured values of rolling resistance coefficient confirm that the rolling resistance for the uneven road is much higher than that for the smooth road surfaces. Particularly, the coefficients of rolling resistance for hard road surfaces are below 0.05, which is much smaller than that predicted for rough runway. It is noted that with regard to hard road surfaces, the rolling resistance is mainly attributed to material hysteresis of tire components. On the other hand, with regard to rough road surface, the longitudinal forces generated on the road unevenness is the major contributor to the total rolling resistance (coefficient of rolling resistance because of longitudinal forces is more than 0.1).

Table 4 Coefficient of rolling resistance for different road surfaces [36]

Road Surface	Coefficient of Rolling resistance
Pneumatic Car tires on	
Large sett pavement	0.015
Small sett pavement	0.015
Concrete, asphalt	0.013
Rolled gravel	0.02
Tarmacadam	0.025
Unpaved road	0.05
Field	0.1-0.35
Pneumatic truck tires on	
Concrete, asphalt	0.006-0.01

4. Conclusion

An approach for developing a detailed finite element tire model using detailed geometry and material property definition was presented. For the transient dynamic properties analysis using finite element explicit program, the road unevenness and material damping were defined to carry out tire rolling simulation, and transient dynamic performance was validated for the tire rolling over different road obstacles. In addition,

Discrete Fourier Transform method, used to generate road unevenness based on the power spectral density of various road surfaces, was presented in this study.

The processes of calculation of rolling resistance generated by the longitudinal dynamic responses on the uneven road were described, where the rolling resistance was defined as energy dissipated per unit distance travelled. In order to predict the effective rolling resistance for this study, a quarter-car model was used, consisting of a tire and a chassis, with suspension in the form of a parallel spring-damper combination connecting the centre of the tire and the chassis. Road length for the effective rolling resistance generation was defined in order to satisfy the requirement of the rolling tire, in which the chassis of the quarter car needs to reach an equilibrium position before it arrived on the uneven road. In addition, transition section and calculation section of the whole road were developed separately, and the effective rolling resistance was derived by calculating the average rolling resistance over the calculation section, which was generated by three revolutions of the rolling tire.

In this study, the simulation was concentrated on rolling resistance generated by the unevenness of the road, and did not account for the rolling resistance generated in the steady state condition (flat road). However, based on the rolling resistance investigation by other researchers [3, 4, 6-8, 30, 36], the material hysteresis is the main contributor to tire rolling resistance in the steady state condition, and it is much smaller when compared to the rolling resistance generated on the uneven road. Thus it can be concluded that the rolling resistance due to transient longitudinal contact forces is the most significant factor for a rolling tire on the uneven road.

References

- [1] A J P Miege, A A Popov. The rolling resistance of truck tyres under a dynamic vertical load. *Vehicle System Dynamics*, 2005, 43(1): 135-144.
- [2] T. G. Ebbott, R. L. Hohman, J. P. Jeusette, and V. Kerchman, Tire Temperature and Rolling Resistance Prediction with Finite Element Analysis. *Tire Sci. and Technol.* 27 (1) (1999) 2-21.
- [3] Z. Shida, M. Koishi, T. Kogure, and K. Kabe, A Rolling Resistance Simulation of Tires Using Static Finite Element Analysis. *Tire Sci. Technol.* 27 (2) (1999) 84-105.
- [4] S. Ghosh, R.A. Sengupta, and G. Heinrich, Investigations on Rolling Resistance of Nanocomposite Based Passenger Car Radial Tyre Tread Compounds Using Simulation Technique. *Tire Sci. Technol.* 39 (3) (2011) 210-222.
- [5] J.R. Cho, K.W. Kimb, D.H. Jeona, W.S. Yooa, Transient dynamic response analysis of 3-D patterned tire rolling over cleat, *Eur. J. Mech. and Solids*, 24 (3) (2005) 519-531.
- [6] J. R. Cho, H. W. Lee, W. B. Jeong, K. M. Jeong, K. W. Kim, Numerical estimation of rolling resistance and temperature distribution of 3-D periodic patterned tire, *Int. J. Solids Struct.* 50 (1) (2013) 86-96.
- [7] J. R. Luchini and James A. Popio, Modeling Transient Rolling Resistance of Tires. *Tire Sci. Technol.* 35 (2) (2007) 118-140.
- [8] S. K. Clark, Rolling Resistance of Pneumatic Tires. *Tire Sci. Technol.* 6 (3) (1978) 163-175.

- [9] P. S. Pillai, Effect of tyre overload and inflation pressure on rolling loss (resistance) and fuel consumption of automobile and truck/bus tires. *Indian Journal of Engineering & Material Science*, 2004, 11: 406-412.
- [10] O. H. Yeoh and P. D. Fleming. A new attempt to reconcile the statistical and phenomenological theories of rubber elasticity. *J. Polym. Sci. B Polym. Phys.*, 35(1997): 1919–1931.
- [11] A. M. Burke and O. A. Olatunbosun, New techniques in tyre modal analysis using MSC/NASTRAN, *Int. j. vehicle Des.* 18 (2) (1997) 203-212.
- [12] X. Yang, O. Olatunbosun, and E. Bolarinwa, Materials Testing for Finite Element Tire Model, *SAE Int. J. Mater. Manuf.* 3(1) (2010) 211-220.
- [13] X. Yang and O.A. Olatunbosun, Optimization of reinforcement turn-up effect on tyre durability and operating characteristics for racing tyre design, *Mater. Des.* 35 (2012) 798–809.
- [14] M. Behroozi, O.A. Olatunbosun and W. Ding, Finite element analysis of aircraft tyre - Effect of model complexity on tyre performance characteristics, *Mater. Des.* 35 (2012) 810-819.
- [15] M. Esgandari and O. Olatunbosun. Computer aided engineering prediction of brake noise: modeling of brake shims. *Journal of Vibration and Control*, 2014: 1077546314547102.
- [16] A. Kamoulakos and B. G. Kao (1998) Transient Dynamics of a Tire Rolling over Small Obstacles — A Finite Element Approach with PAMSHOCK. *Tire Sci.Technol.* 26 (2) (1998) 84-108.
- [17] M. Koishi, K. Kabe, and M. Shiratori (1998) Tire Cornering Simulation Using an Explicit Finite Element Analysis Code. *Tire Sci.Technol.* 26 (2) (1998) 109-119.
- [18] P. Ghosh, A. Saha, P.C. Bohara, and R. Mukhopadhyay. Material property characterization for finite element analysis of tires. *Rubber World*, 233(4) (2006)
- [19] Abaqus Example Problems Manual. DassaultSystemes. Abaqus 6.10.
- [20] O. H. Yeoh, On the Ogden Strain-Energy Function. *Rubber Chem. Technol.* 70 (2) (1997) 175-182.
- [21] ASTM D412-06a, Standard Test Methods for Vulcanized Rubber and Thermoplastic Elastomers—Tension. 2006
- [22] Man Liu, and D.G. Gorman, Formulation of Rayleigh damping and its extensions. *Comput. & Struct.* 57 (2) (1995) 277–285.
- [23] Xucheng Wang, *Finite Element Method*, Tsinghua University Press. 2003.
- [24] S.Arabi, O.A. Olatunbosun, and M. Behroozi, Development of Virtual Testing of EGR Coolant Rail. *SAE Int. J. Passeng. Cars - Mech. Syst.*, 2013. 6(2): p. 927-936.
- [25] O. A. Olatunbosun and A. M. Burke, Finite Element Modelling of Rotating Tires in the Time Domain. *Tire Sci.Technol.* 30 (1) (2002) 19-33.
- [26] P. Bandel and C. Monguzzi, Simulation Model of the Dynamic Behavior of a Tire Running Over an Obstacle. *Tire Sci.Technol.* 16 (2) (1988) 62-77.
- [27] C. W. Mousseau and S. K. Clark, An Analytical and Experimental Study of a Tire Rolling Over a Stepped Obstacle at Low Velocity. *Tire Sci. Technol.* 22 (3) (1994) 162-181.
- [28] C.W. Mousseau, G.M. Hulbert, An efficient tire model for the analysis of spindle forces produced by a tire impacting large obstacles, *Comput. Methods Appl. Mech. Eng.* 135 (1-2) (1996) 15–34.
- [29] C.Weï and O.A. Olatunbosun, Transient dynamic behaviour of finite element tire traversing obstacles with different heights. *Journal of Terramechanics*, 2014, 56: 1-16.
- [30] M. A. Lak, G. Degrande and G. Lombaert. The effect of road unevenness on the dynamic vehicle response and ground-borne vibrations due to road traffic. *Soil Dynamics and Earthquake Engineering.* 31(10), 2011.1357-1377.
- [31] J. Y. Wong, *Theory of Ground Vehicles*, Third Edition, 2001
- [32] A. V. Oppenheim and R. W. Schaffer, *Discrete-Time Signal Processing*, Prentice Hall c1989
- [33] V. Kerchman, Tire-Suspension-Chassis Dynamics in Rolling over Obstacles for Ride and Harshness Analysis. *Tire Sci. Technol.* 36 (3) (2008) 158-191.
- [34] Grzegorz Litak, Marek Borowiec, Michael I. Friswell and Kazimierz Szabelski. Chaotic vibration of a quarter-car model excited by the road surface profile. *Commun. Nonlinear Sci. Numer. Simul.* 13 (7) (2008) 1373-1383.
- [35] Hugh Jack, *Dynamic System Modeling and Control*, 2005
- [36] Robert Bosch GmbH, *Automotive Handbook*, 2002